PHYSICAL REVIEW B **78**, 184108 (2008)

First-principles study of microscopic properties of the Nb antisite in $LiNbO_3$: Comparison to phenomenological polaron theory

H. H. Nahm* and C. H. Park†

Research Center for Dielectric and Advanced Matter Physics and Department of Physics, Pusan National University, Busan 609-735, Republic of Korea

(Received 18 June 2008; revised manuscript received 7 October 2008; published 17 November 2008)

Through the first-principles local-density-approximation+Hubbard-U (LDA+U) electronic-structure calculation method, the microscopic properties of the Nb antisite (Nb_{Li}) and the electron-lattice interaction are investigated. The atomic structure is found to depend on the capture of electrons at the defect level, and especially when the defect level is occupied by two electrons, the Nb_{Li} undergoes a large-lattice-relaxation (LLR), accompanied with the formation of the deep level. The main driving force toward the LLR is suggested to be the orbital hybridization of the defect level state and the conduction-band state. As a result, the Nb_{Li} defect exhibits a negative-U property. Based on the computational results, several well-known light-induced phenomena in $LiNbO_3$ and the polaron model are discussed.

DOI: 10.1103/PhysRevB.78.184108 PACS number(s): 61.72.Bb, 61.72.J−, 61.80.Ba

It is well-known that the optical properties of $LiNbO_3$ (LNO) such as refractivity and absorption spectrum are changed by the light illumination.[1,2] The photoinduced refractivity (PR) has been extensively investigated[1,3–7] since it can be employed in fabricating the nonvolatile holographic memory. The PR has been observed also in several perovskite structured oxides such as $KNbO_3$ (Ref. 8) and $BaTiO_3$,[9] and other oxides such as $KTiOP_4$ (Ref. 10) and LiB_3O_5.[11] Special attention has been paid to the PR of $LiNbO_3$ since the large homogenous crystal is available and the PR effect is strong and robust at room temperature.[1,3,4,12] A remarkable observation is that the two-color illumination using both green-blue and infrared (IR) lights can cause strong and robust PR even in the undoped $LiNbO_3$.[3,4] Other important light-induced phenomena in $LiNbO_3$ are the enhancement of the IR absorption of $LiNbO_3$ after the green light illumination[5,6] and the enhancement of the visible and IR absorptions after ultraviolet (UV) illumination.[7] It is suggested that these photoinduced effects may have a similar origin.

The as-grown $LiNbO_3$ is usually Li deficient (congruent).[13–15] Many experimental measurements[1] and theoretical calculations[16,17] indicated that Nb antisite (Nb_{Li}) as well as Li vacancy (V_{Li}) is dominant in the congruent $LiNbO_3$, and they compensate each other.[17] The Nb_{Li} is indicated to be responsible for the PR by experimental data such as optical-absorption spectrum and the growth condition dependence.[4,6]

A polaron model,[18,19] based on antisite Nb_{Li} and on-site Nb_{Nb}, is suggested to explain the microscopic mechanisms of these photoinduced phenomena including the PR in $LiNbO_3$ and the two-color method. The polaron indicates a quasiparticle state of charge carriers which are trapped by the lattice displacements of the neighbors. In $LiNbO_3$, the several polaron states have been observed. The role of the polarons bound at the antisite defect Nb_{Li} (bound small polaron and bipolaron) and the free small polaron bound at Nb_{Nb} is suggested to be important for the understanding of the PR process. The bipolaron state and metastable bound small-polaron state were indicated by the broad peak in absorption spectrum at around 2.5 eV (Refs. 4 and 20) and the photoexcited peak at around 1.6 eV,[19,21] respectively. On the other hand, a free small polaron at on-site Nb_{Nb} atoms was indicated by a peak at 1.0 eV.[19,22] The stable bipolaron states are reported to be easily formed in thermal reduction process at high T above 850 K.[20] The small-polaron state is measured through the light illumination, and therefore indicated to be a metastable state. The photoinduced metastable phenomena of $LiNbO_3$ are successfully explained based on these polarons; however the microscopic structures of these polaron states around the antisite defect Nb_{Li} are not clearly resolved yet. Therefore, in this work, we investigate the microscopic properties of Nb_{Li} in $LiNbO_3$ and the electron-lattice interaction through the first-principles electronic-structure calculations. We show that a large-lattice relaxation (LLR) at the Nb_{Li} defect can be induced by the capture of electrons at the defect level, and the driving mechanism is the interaction between the electrons at the defect level and the empty conduction-band states.

Our calculations were performed with the projector-augmented-wave (PAW) pseudopotentials[23] by using Vienna *Ab initio* Simulation Package (VASP) code[24] on the basis of both local-density-approximation (LDA) and LDA+U methods.[25] The wave functions were expanded in a plane-wave basis set with an energy cutoff of 400 eV. We used standard PAW potentials in the VASP distribution. The 4p and 4d orbitals for Nb atom and the 1s orbital for Li atom are explicitly included in the calculations. In order to simulate the defect, we use a $(2\times2\times2)$ rhombohedral supercell including 80 atoms. All atomic positions were fully relaxed until the Hellmann-Feynman force on each atom was reduced within 0.01 eV/Å. The k-space integration was performed by $(4\times4\times4)$ mesh points. The optimized structural parameters and the bulk modulus of the pure rhombohedral $LiNbO_3$ calculated by LDA and LDA+U methods are shown in Table I. The calculated lattice constants and the angle between lattice vectors of the rhombohedral structure in Fig. 1(a) are in good agreement with the experimental values.[26] The band gap (E_g) is calculated to be 3.35 eV at a zone center (Γ) of Brillouin zone by LDA,[27] which is underesti-

TABLE I. The structural parameters of a ferroelectric rhombohedral ten atoms supercell $LiNbO_3$ calculated by LDA and LDA+U methods (the values of $U'=U-J$ in the unit of electron volts are indicated below) are shown. Here, B is a bulk modulus (unit: Mbar). $d_{\text{Nb-Nb}}$, $d_{\text{Nb-O}}$, and $d_{\text{Li-O}}$ are the nearest (second-nearest) distances between the atoms indicated by subscripts (unit: angstroms).

	a	θ	B	$d_{\text{Nb-Nb}}$	$d_{\text{Nb-O}}$	$d_{\text{Li-O}}$
LDA	5.461	55.61	1.118	3.734	1.900(2.104)	2.004(2.219)
$U'=3$	5.475	55.68	1.166	3.746	1.939(2.071)	1.989(2.275)
$U'=4$	5.483	55.70	1.194	3.753	1.952(2.063)	1.979(2.293)
$U'=5$	5.493	55.71	1.224	3.759	1.964(2.056)	1.972(2.316)
Exp[a]	5.494	55.52	1.154	3.765	1.889(2.112)	2.068(2.238)

[a]Experimental data of Ref. 26.

mated compared to the experimental value of 3.78 eV (Ref. 28) due to the well-known LDA shortcoming.[29]

At first, the electron-lattice interaction in the Nb_{Li}^{5+} is investigated. In the Nb_{Li}^{5+}, a monovalent Li^+ atom is replaced by a Nb^{5+} atom with five valence electrons, as shown by Fig. 1(b), and thus Nb_{Li} is expected to be stable *in the* (4+)-charge state as a quadruple donor [$Nb_{Li}^{(4+)}$ in Kröger Vink notation but here denoted by $Nb_{Li}^{5+}(4d^0)$ to emphasize that the defect 4*d*-driven state is empty]. It is found that the Nb_{Li}^{5+} makes three *empty* (nearly-degenerate) shallow defect levels near the conduction-band minimum (CBM): two degenerate levels and one slightly upper level, which are located, respectively, at 0.06 eV below CBM and nearly at CBM by LDA calculation. When one electron is captured by a defect level, i.e., in the (3+)-charge state [denoted by $Nb_{Li}^{4+}(4d^1)$], the atomic structures are slightly changed, and the atomic distance between an Nb_{Li} and a nearest Nb_{Nb} atom (which is located along the direction of ferroelectric polarization from the Nb_{Li}, i.e., the [0001] direction in the hexagonal structure or the [111] direction in the rhombohedral structure), $d_{\text{Nb-Nb}}^{[111]}$, becomes smaller slightly from 3.08 (at Nb_{Li}^{5+}) to 3.04 Å (at Nb_{Li}^{4+}). An important finding is that when the antisite level is occupied by two electrons, i.e., in the (2+)-charge state [denoted by $Nb_{Li}^{3+}(4d^2)$], the electron-lattice interaction around the Nb_{Li} becomes much more significant and the Nb_{Li} undergoes a LLR. Here both a Nb_{Li} and a nearby on-site Nb_{Nb} are seriously attracted toward each other, as described by Fig. 1(c). The atomic distance between two Nb atoms, $d_{\text{Nb-Nb}}^{[111]}$, is greatly reduced by 0.36 Å, compared to Nb_{Li}^{5+}, in which the displacement of the Nb_{Li} (0.24 Å) is about twice larger than that of the Nb_{Nb} (0.12 Å). We would note that the $Nb_{Li}^{3+}(4d^2)$ is more accurately described by $Nb_{Li}^{4+}(4d^1)$-$Nb_{Nb}^{4+}(4d^1)$ since two electrons are captured by a covalent-bonding-like orbital formed between two Nb atoms, which will be discussed below as shown by Fig. 3(c). This seems to be consistent with bipolaron, which can be described as a strong-coupling state of a bound small polaron and a free small polaron.

The electronic structure is significantly changed, accompanied with the lattice relaxation. The electronic structures of the Nb_{Li} calculated by LDA+U are shown in Fig. 2 and the defect level estimated by both LDA and LDA+U methods are shown in Table II. In Table III, the atomic displacements of several Nb atoms around the Nb_{Li} are described. In the $Nb_{Li}^{4+}(4d^1)$, the electronic structure is also slightly changed from $Nb_{Li}^{5+}(4d^0)$, and a defect level is slightly lowered (by 0.05 eV by LDA); however, in the $Nb_{Li}^{3+}(4d^2)$, the defect level becomes significantly deeper through the LLR. These indicate the strong electron-lattice interaction in Nb_{Li}.

The changes of the wave function of the defect level of Nb_{Li} according to the electron capture are described in Fig. 3. The defect levels of Nb_{Li} are characterized mainly by the

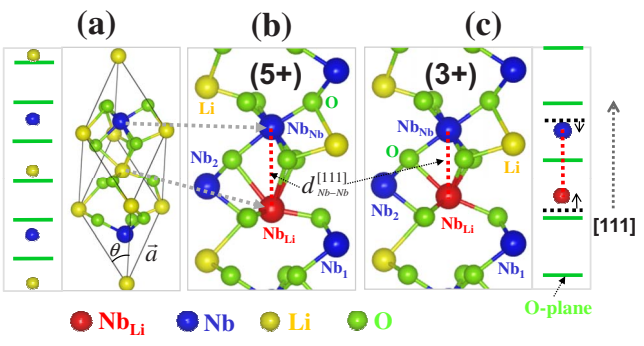

FIG. 1. (Color online) The atomic structures of (a) the pure ferroelectric $LiNbO_3$, (b) the $Nb_{Li}^{5+}(4d^0)$, and (c) the LLR-$Nb_{Li}^{3+}(4d^2)$ in hexagonal and rhombohedral structures are described. The distance of Nb_{Li} and Nb_{Nb} ($d_{\text{Nb-Nb}}^{[111]}$) is much smaller in the Nb_{Li}^{3+} than in the Nb_{Li}^{5+}, along a [111]([0001]) direction of ferroelectric polarization. The (green online) lines describe [111] oxygen planes.

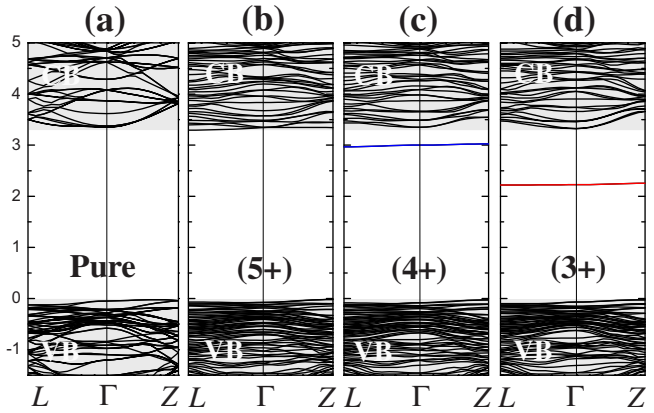

FIG. 2. (Color online) The electronic structures of (a) pure, (b) $Nb_{Li}^{5+}(4d^0)$, (c) $Nb_{Li}^{4+}(4d^1)$, and (d) $Nb_{Li}^{3+}(4d^2)$ are shown by using the LDA+U calculations ($U'=4.0$ eV). Here, $L=(0,\frac{1}{2},0)$, $\Gamma=(0,0,0)$, and $Z=(\frac{1}{2},\frac{1}{2},\frac{1}{2})$.

TABLE II. The band gap E_g, the Nb_{Li}-Nb_{Nb} distance $d^{[111]}_{Nb\text{-}Nb}$ around Nb_{Li}, the defect level ϵ_D of the q-charged Nb_{Li} for $q=(5+)$, $(4+)$, and $(3+)$ (relative to CBM) are shown. The level of Nb^{3+}_{Li} is sensitively changed by U'. The reaction energy ΔE of Eq. (1) calculated by LDA and LDA+U methods are also shown. The positive value of ΔE describe the negative-U character of Nb_{Li} (see text).

		$d^{[111]}_{Nb\text{-}Nb}$ (Å)			ϵ_D (eV)			
	E_g (eV)	Nb^{5+}_{Li}	Nb^{4+}_{Li}	Nb^{3+}_{Li}	Nb^{5+}_{Li}	Nb^{4+}_{Li}	Nb^{3+}_{Li}	ΔE (eV)
LDA	3.35	3.081	3.049	2.707	−0.06	−0.11	−0.61	0.14
$U'=3$	3.36	3.040	2.910	2.646	−0.08	−0.21	−0.83	0.47
$U'=4$	3.46	3.032	2.890	2.639	−0.09	−0.34	−1.11	0.57
$U'=5$	3.59	3.026	2.878	2.638	−0.09	−0.49	−1.42	0.68
Cal[a]	3.80					−1.40	−1.66	
Exp[b]	3.78[c]							0.27[d]

[a]Other calculation: Ref. 16.
[b]Experimental data.
[c]Reference 28.
[d]Reference 18.

Nb_{Li}-4d orbital and localized around the Nb_{Li} atom in Nb^{5+}_{Li} state. By the LLR in $Nb^{3+}_{Li}(4d^2)$, the defect orbital is extended to a nearest Nb_{Nb} atom and a covalent-bonding-like orbital localized between a Nb_{Li} and a Nb_{Nb} is formed. The defect level of Nb^{3+}_{Li} is deeply located within the band gap, as shown in Fig. 2(d). The on-site Coulomb interaction at the localized Nb-4d orbitals is expected to be strong. It is suggested that the LDA+U method helps the more accurate description of the localized level. A self-electron-interaction (SI) energy is an artifact in the LDA calculations, and it is known to be serious for the localized 4d orbital. In the LDA+U method, the error by the SI is forced to be reduced by the value of a parameter $Nb^{3+}_{Li}(4d^2)$. A problem of current LDA+U method, the U value, which can effectively compensate the SI energy, cannot be accurately determined. Therefore, we give the computational results by several assumed values of $U'=U-J$ of Nb-4d orbitals. The location of defect level and the band gap estimated by various U' values are compared in Table II. It is noted that the localized defect level of $Nb^{3+}_{Li}(4d^2)$ state capturing two electrons is sensitively changed by the U' value of LDA+U method, indicating that the orbital of this level is seriously localized between two Nb atoms. The main results of the atomic structures by LDA+U calculations are similar to those by LDA. The atomic distance, $d^{[111]}_{Nb\text{-}Nb}$, in the LLR-$Nb^{3+}_{Li}(4d^2)$ becomes slightly reduced from 2.707 Å by LDA to 2.639 Å by LDA+U ($U'=4$ eV).

TABLE III. The atomic positions $(a,b,c)=a\vec{R}_a+b\vec{R}_b+c\vec{R}_c$ of Nb atoms around the original Li atom in pure $LiNbO_3$ or Nb_{Li} atom are given in the lattice-vector coordinates of a 80 atoms rhombohedral supercell [$\vec{R}_a=A(\alpha,\alpha,\beta)$, $\vec{R}_b=A(\alpha,\beta,\alpha)$, and $\vec{R}_c=A(\beta,\alpha,\alpha)$ where $A=3.8579$ Å, $\alpha=2.0$, and $\beta=0.1331$]. Furthermore, the changes of the atomic positions $(\delta a,\delta b,\delta c)$ in $Nb^{4+}_{Li}(4d^1)$ and $Nb^{3+}_{Li}(4d^2)$ states are also given, relatively to the corresponding positions of Nb^{5+}_{Li}. Here, Nb_{Nb} is nearest Nb located along [111] direction, and Nb_1 and Nb_2 are three equivalent Nb and other three equivalent Nb, respectively (see Fig. 1).

	Pure $LiNbO_3$ (a,b,c)	Nb^{4+}_{Li} $(\delta a,\delta b,\delta c)\times 100$
Li (Nb_{Li})	(0.00000, 0.00000, 0.00000)	(0.32, 0.32, 0.32)
Nb_{Nb}	(0.10722, 0.10722, 0.10722)	(−0.19, −0.19, −0.19)
Nb_1	(0.10722, 0.60722, 0.10722)	(0.10, 0.31, −0.24)
Nb_2	(0.85722, 0.35722, 0.85722)	(−0.05, −0.13, 0.07)

	Nb^{5+}_{Li} (a,b,c)	Nb^{3+}_{Li} $(\delta a,\delta b,\delta c)\times 100$
Nb_{Li}	(0.00000, 0.00000, 0.00000)	(0.87, 0.87, 0.87)
Nb_{Nb}	(0.10977, 0.10977, 0.10977)	(−0.55, −0.55, −0.55)
Nb_1	(0.10164, 0.58862, 0.11401)	(0.15, 0.76, −0.51)
Nb_2	(0.84643, 0.37553, 0.84120)	(−0.17, −0.05, −0.05)

The LLR through electron capture can be understood to be driven by the hybridization of an electron-occupied Nb_{Li}-defect level and an unoccupied orbital of on-site Nb_{Nb} atom whose energy is located above CBM. As the Nb_{Li} atom is displaced toward a Nb_{Nb} atom located along the [111]-polarized direction (see Fig. 1), the 4d orbitals of two Nb

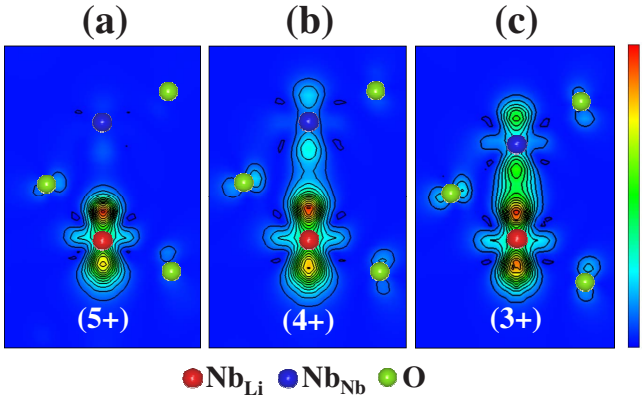

FIG. 3. (Color online) The wave functions of the lowest defect level are displayed on a $[2\bar{1}\bar{1}]$ plane for (a) $Nb^{5+}_{Li}(4d^0)$, (b) $Nb^{4+}_{Li}(4d^1)$, and (c) $Nb^{3+}_{Li}(4d^2)$. The interval between contour lines is 0.1e per 80 atoms rhombohedral supercell.

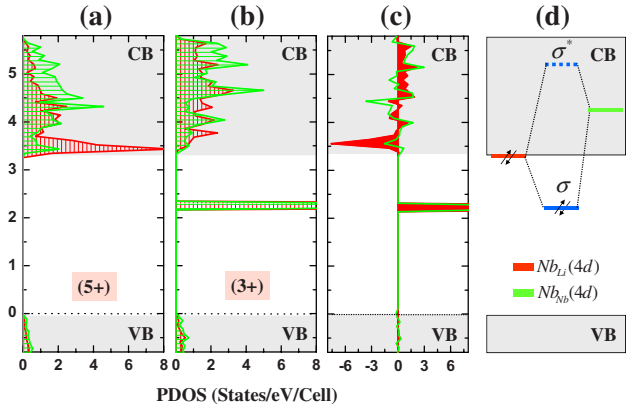

FIG. 4. (Color online) The PDOS of the $4d$ orbitals of an antisite Nb_{Li} atom and a Nb_{Nb} atom near the Nb_{Li} in (a) $Nb_{Li}^{5+}(4d^0)$ and (b) $Nb_{Li}^{3+}(4d^2)$ are shown. (c) The differences between two PDOSs of (a) and (b) are displayed. The zero energy denotes the valance band maximum. (d) The stabilized mechanism of the LLR is schematically displayed. Here, arrow is an electron with a spin direction.

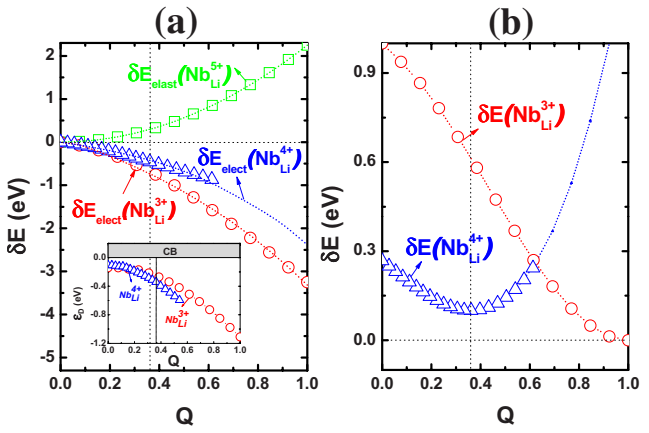

FIG. 5. (Color online) (a) The variation in the total energies of $Nb_{Li}^{4+}(4d^1)$ and $Nb_{Li}^{3+}(4d^2)$ according to the atomic displacements, Q, is divided to the variations of the elastic component δE_{elast} and the electronic energy component δE_{elect}. In the inset, the variation in the defect levels ϵ_D versus Q is shown. (b) The variations of the total energies of $Nb_{Li}^{4+}(4d^1)$ and $Nb_{Li}^{3+}(4d^2)$ versus Q, aligned by using the reaction energy of Eq. (1), are shown. The vertical dotted line describes the Q of the stable geometry of $Nb_{Li}^{4+}(4d^1)$ relative to the displacement of $Nb_{Li}^{3+}(4d^2)$. (Colored) dot lines denote the fitting curve.

atoms interact with each other, which makes the lowest defect level of $4d$ orbitals mainly by the Nb_{Li} *lowered* and the energy levels of the on-site Nb_{Nb} *raised*. In order to understand the interaction between two Nb atoms, we compared the partial density of states (PDOS) of the Nb-$4d$ from the antisite Nb_{Li} atom and the nearest Nb_{Nb} between $Nb_{Li}^{5+}(4d^0)$ and LLR-$Nb_{Li}^{3+}(4d^2)$ states, as shown in Fig. 4. It is clearly shown that the energies of the on-site Nb_{Nb}-$4d$ orbitals are raised while the defect level from the antisite Nb_{Li} atom is significantly lowered by the atomic displacements in $Nb_{Li}^{3+}(4d^2)$. It indicates that there is a strong interaction between two Nb-$4d$ orbitals, by which the lower level is decreased. When the lower defect level has electrons in Nb_{Li} [one in $Nb_{Li}^{4+}(4d^1)$ and two in $Nb_{Li}^{3+}(4d^2)$], the electronic energy of defect can be decreased by the displacement, which derives the lattice relaxation. On the other hand, the elastic energy is increased by the atomic displacement, which balances the electronic energy reduction. As more electrons are occupied at the defect level, the reduction in the electronic energy becomes larger, and thus the larger lattice relaxation is induced. Furthermore the defect level becomes deeper, as in the case of the $Nb_{Li}^{3+}(4d^2)$. The formation of the molecular covalent-bonding orbital between the Nb_{Li} and Nb_{Nb} has been predicted earlier.[16,18] This is now nicely proved by the present results.

The contribution to the change of total energy by the lattice distortion can be described mainly by two factors: (i) the quantum-mechanical electronic component and (ii) the elastic component. The former comes from the orbital hybridization. It can be explained by exponential function as shown below. We estimated the contributions of the elastic energy and the electronic energy to the change of the total energy by the lattice relaxation, as follows: (i) Firstly, we calculated the total energies of the several lattice structures generated by interpolating two atomic structures of $Nb_{Li}^{5+}(4d^0)$ as an on structure ($Q=0$) and $Nb_{Li}^{3+}(4d^2)$ as a LLR off structure ($Q=1$). The interpolation parameter Q describes the lattice relaxation. (ii) The elastic energy variation is estimated by the total-energy variation, $\delta E(Q)=E(Q)-E(0)$, calculated for the $Nb_{Li}^{5+}(4d^0)$. Since the defect level has no electron, the electronic contributions can be neglected. The result is shown by δE_{elast} in Fig. 5(a). The variation in the elastic energy component follows $\frac{1}{2}KQ^2$ with $K=11.4$. (iii) Now, the electronic part, i.e., the contributions of the captured electrons to the lattice relaxation energies in $Nb_{Li}^{4+}(4d^1)$ and $Nb_{Li}^{3+}(4d^2)$, can be estimated by the difference in the total-energy variations of these states and Nb_{Li}^{5+}: $\delta E(Q;Nb_{Li}^{q}) - \delta E(Q;Nb_{Li}^{5+})$. This electronic component is found to be well described by an exponential function of $A[1-\exp(BQ)]$: for $Nb_{Li}^{3+}(4d^2)$, $A=1.7062$ and $B=1.0985$ and for $Nb_{Li}^{4+}(4d^1)$, $A=0.43395$ and $B=1.87069$ (see Fig. 5). When Q is small, the variation in electronic energy can be described by VQ, where V is A^*B, and it is similar to the electron-phonon interaction formula in the phenomenological polaron theory.[30] The exponential behavior indicates the effect of the orbital hybridization between the Nb_{Li} and Nb_{Nb} atoms induced by the atomic displacement. In the inset of Fig. 5(a), the variation in the defect level depending on Q is described, which is also exponentially changed, similarly to the change of the electronic component. These results indicate that the driving force of the LLR is the hybridization between the electron-occupied defect level at the Nb_{Li} and the empty orbitals of a nearby Nb_{Nb} atom. The variation in the electronic energies of the $Nb_{Li}^{4+}(4d^1)$, having one electron at the defect level, is slightly larger than the half of $Nb_{Li}^{3+}(4d^2)$, having two electrons at the defect level, since the electronic energy reduction by the lattice relaxation is compensated by the increased electron-electron repulsive interaction by the LLR because the lattice displacement makes the defect orbital more strongly localized.

Through the LLR, the Nb_{Li} defect becomes a negative-U center. We examined the next reaction:

$$2\mathrm{Nb}_{\mathrm{Li}}^{4+}(4d^1) \rightarrow \mathrm{Nb}_{\mathrm{Li}}^{3+}(4d^2) + \mathrm{Nb}_{\mathrm{Li}}^{5+}(4d^0) + \Delta E. \quad (1)$$

The reaction is calculated to be exothermic. The right side is more stable by 0.14 eV (ΔE) by LDA calculations. These indicate that *the* $\mathrm{Nb}_{\mathrm{Li}}^{4+}(4d^1)$ is a metastable state, and thus the $\mathrm{Nb}_{\mathrm{Li}}$ should be diamagnetic and inactive to the electron-spin-resonance (ESR) measurement (can be activated by light), which agrees with the experimental results.[5,31] The negative-U property of the $\mathrm{Nb}_{\mathrm{Li}}$ originates from the compensation for the repulsive Coulombic interaction energy at the defect level by the electronic energy reduction through the LLR. The negative-U reaction energy of Eq. (1) is calculated to be larger (linearly to the value of $U'=U-J$) by the LDA+U calculations, as shown by Table II, because the LDA+U method makes the artificial Coulombic repulsive self-interaction energy at the defect orbital, especially at the localized orbital of $\mathrm{Nb}_{\mathrm{Li}}^{3+}(4d^2)$, smaller. The thermal dissociation energy of the bipolaron state into the small-polaron state was measured to be 0.27 eV.[18,20] This is consistent with the ΔE estimated by the LDA+U method with $U'=1.2$ eV which is inferred by a linear interpolation of data in Table II. The negative-U property indicates that two states of $\mathrm{Nb}_{\mathrm{Li}}^{3+}(4d^2)$ and $\mathrm{Nb}_{\mathrm{Li}}^{5+}(4d^0)$ coexist.

In respect that $\mathrm{Nb}_{\mathrm{Li}}^{3+}(4d^2)$ and $\mathrm{Nb}_{\mathrm{Li}}^{4+}(4d^1)$, respectively, capture two and one electrons at the defect level, they are consistent with the bipolaron and the bound small polaron. The metastable $\mathrm{Nb}_{\mathrm{Li}}^{4+}(4d^1)$ is consistent with the bound small polaron in respect that the bound small polarons are metastably generated by the light illumination. The light-induced bound small polaron indicated by the absorption peak at around 1.6 eV has a finite lifetime which is suggested to be of the order of ~milliseconds at room temperature[19] and can be much longer at low temperature. Recently, Merschjann *et al.*[19] carefully analyzed the relaxation process of the photoexcited small polarons and they found that there are two kinds of process: *slow* and *fast* relaxations with the activation energies of 0.57 and 0.20 eV which were explained by the excitation of electron from the bound small polaron to free small polaron, and the energy barrier for free small-polaron hopping, respectively. Based on the present computational results, the metastable bound small polaron can be relaxed by the transition to the more stable $\mathrm{Nb}_{\mathrm{Li}}^{3+}(4d^2)$ or $\mathrm{Nb}_{\mathrm{Li}}^{5+}(4d^0)$. These can occur either by $\mathrm{Nb}_{\mathrm{Li}}^{4+}(4d^1) \rightarrow \mathrm{Nb}_{\mathrm{Li}}^{5+}(4d^0) + e$ or by $\mathrm{Nb}_{\mathrm{Li}}^{4+}(4d^1) + e \rightarrow \mathrm{Nb}_{\mathrm{Li}}^{3+}(4d^2)$. In Ref. 19, the latter transition was explained by the capture of an electron of free small-polaron state at the bound small polaron, for which the small energy barrier for the hopping of free small polarons is suggested to lead a fast relaxation. The former transition requires a larger energy for the excitation of the electron at the deep level of $\mathrm{Nb}_{\mathrm{Li}}^{4+}(4d^1)$ to the free small-polaron state, which is consistent with the slow relaxation with a large activation energy. The energy level of the $\mathrm{Nb}_{\mathrm{Li}}^{4+}(4d^1)$ is calculated to be located at 0.49 eV below CBM (assuming the $U'=5$ eV in Table II, if a large U is used, the level is estimated to be lower) which is comparable to the large activation energy of 0.57 eV. It is also consistent with the experimental measurement of the binding energy of the bound small polaron of 0.62 eV from the conductivity measurement.[18] For more detailed understanding of the relaxation, the free small polaron should be understood since the electron at bound small polaron can be excited more easily to the lower energy state, which can be a free small-polaron state rather than the CBM state. If the concentration of $\mathrm{Nb}_{\mathrm{Li}}$ is rich, the electron of $\mathrm{Nb}_{\mathrm{Li}}^{4+}$ can be excited to the empty defect level of $\mathrm{Nb}_{\mathrm{Li}}^{5+}$.

Berben *et al.*[32] found that the depopulation of small polarons shows a stretched exponential behavior and suggested that the lifetime of an individual small polaron depends on the distance to the next deep trap. The lifetime was reported to depend on the Li deficiency and it changes from <40 ms in the congruent $LiNbO_3$ to ~400 ms in near-stoichiometric $LiNbO_3$, which may be understood from the view that the reactions between the photoexcited $\mathrm{Nb}_{\mathrm{Li}}^{4+}$ defects, which generates the more stable $\mathrm{Nb}_{\mathrm{Li}}^{3+}$ and $\mathrm{Nb}_{\mathrm{Li}}^{5+}$, should be the more active as the concentration of the $\mathrm{Nb}_{\mathrm{Li}}$ is higher and the average distance between $\mathrm{Nb}_{\mathrm{Li}}^{4+}$ defects is closer.

We compare furthermore the computational results for the defect levels with the experimental data suggested for the bipolaron and small bound polaron at $\mathrm{Nb}_{\mathrm{Li}}$. The deep defect level of the former LLR state and the intermediate level of $\mathrm{Nb}_{\mathrm{Li}}^{4+}(4d^1)$ are comparable with the energy levels of the deep bipolaron and the intermediate small-polaron level, indicated by the absorption spectra centered at 2.5 and 1.6 eV,[22] respectively. The average levels of the polaron states relative to CBM are not yet clearly measured. Instead, we would note that the difference between defect levels of $\mathrm{Nb}_{\mathrm{Li}}^{3+}(4d^2)$ and $\mathrm{Nb}_{\mathrm{Li}}^{4+}(4d^1)$ is about 0.77–0.93 eV by LDA+U calculations with $U'=4-5$ eV, which is indirectly comparable to the difference of about 0.9 eV in the positions of the absorption peaks both from the bound small polaron and from the bipolaron. For the full understanding of the optical absorptions of small polarons and bipolaron, the excited final levels must be known and Franck-Condon (F-C) shift should be considered. Moreover, the F-C shift, which is determined by the electron-lattice interaction, should be quite strong for the bound polaron states, and also should be quite different for bound small polaron and bipolarons. Therefore the difference in absorption peaks and that in the electronic levels are, here, only indirectly compared. A previous theoretical study has indicated the existence of the bipolaron and bound small-polaron states at 1.66 and 1.40 eV below CBM, respectively.[16]

The well-known polaron model for the mechanisms of the light-induced effects in $LiNbO_3$ (Refs. 16 and 33) can be revisited with the computational results for the microscopic structure of the $\mathrm{Nb}_{\mathrm{Li}}$ since the polaron model is based on the bipolaron and the metastable small polaron, which are correlated to the $\mathrm{Nb}_{\mathrm{Li}}^{3+}(4d^2)$ and $\mathrm{Nb}_{\mathrm{Li}}^{4+}(4d^1)$, respectively. We, now, discuss the polaron model of the PR enhanced by the two-color illumination. The negative-U property indicates that two states of $\mathrm{Nb}_{\mathrm{Li}}^{3+}(4d^2)$ and $\mathrm{Nb}_{\mathrm{Li}}^{5+}(4d^0)$ can coexist since $\mathrm{Nb}_{\mathrm{Li}}^{4+}(4d^1)$ is metastable. The ratio of their concentrations should depend on the presence of other defects such as Li vacancy. According to the polaron model, the carriers are localized at the bipolaron states, and then the light illumination excites the carriers and the bipolarons are transformed into the bound small polarons,[16,33] i.e., the bipolaron states are removed by light excitations.[3,4,12,19] The small polaron is metastable and can return to the original more stable bipolaron state, as discussed above. The two-color illumination

method has an advantage since both bipolaron and the excited small polaron are efficiently eliminated by two colors: an electron of the deep bipolaron state can be excited by the high-energy blue-green photon, and the resulting small-polaron state can be efficiently eliminated by the low-energy IR. The latter process can be also induced by the high-energy photon but the use of low-energy photon is more efficient since the low-energy IR is absorbed only by $Nb_{Li}^{4+}(4d^1)$. The resulting free electrons can move from the illuminated area to the dark area, where they can be captured by the $Nb_{Li}^{5+}(4d^0)$, which can then be transformed into the bipolaron state. As a result, the carriers are distributed by charge transfer from the illuminated region into the dark region and the PR, i.e., the Nb_{Li}^{5+} state is rich in illuminated region and Nb_{Li}^{3+} state is rich in dark region. Since these light-induced imbalance is metastable, the state should be thermal equilibrated, for which electrons at Nb_{Li}^{3+} are excited to free small-polaron state or CBM state.

There are other photoinduced optical properties of $LiNbO_3$ which were explained by the polaron model:[6,7,19] (i) the green-induced IR absorption accompanied with the bleaching of green-absorption[6] and (ii) the UV-induced IR (or visible) absorption.[7] The LLR-$Nb_{Li}^{3+}(4d^2)$ capturing two electrons at the defect level can be excited into $Nb_{Li}^{4+}(4d^1)$ having one electron by the illumination of green light. It results in the elimination of the deep levels of the LLR structure, that is, the elimination of bipolaron, and the temporary increase in the concentration of the metastable $Nb_{Li}^{4+}(4d^1)$ (small polaron). The former and the latter are responsible for the bleaching of green absorption and the increased IR absorption, respectively. Next, the illumination of UV light generates electrons at conduction bands. The electrons can be captured by the $Nb_{Li}^{5+}(4d^0)$ [and then by $Nb_{Li}^{4+}(4d^1)$]. These can induce the processes: $Nb_{Li}^{5+}(4d^0) \rightarrow Nb_{Li}^{4+}(4d^1)$ $[Nb_{Li}^{4+}(4d^1) \rightarrow Nb_{Li}^{3+}(4d^2)]$, which is responsible for the temporal increase in the IR (or visible) absorption. The photoinduced state should be finally thermally equilibrated through the reaction of Eq. (1).

In summary, we investigate the microscopic structure and the electronic structure of the Nb_{Li} in $LiNbO_3$ depending on the charge state. It is found that as the defect level is occupied by electrons, the Nb_{Li} defect undergoes a large-lattice relaxations. The main driving mechanism is suggested to be the quantum-mechanical hybridization between the electron-occupied defect level characterized by the $4d$ orbitals of antisite Nb_{Li} atom and the electron-empty conduction-band states by the $4d$ orbitals of the on-site Nb_{Nb} atoms. It is shown that the well-known several photoinduced changes in the optical property of $LiNbO_3$ can be explained in respect of the large light-induced change in the lattice structure and the electronic structure.

This work was supported by Korea Research Foundation Grant (No. KRF-2006-005-J02804).

*hnam@pusan.ac.kr
†cpark@pusan.ac.kr

[1] P. Gunter and J.-P. Huinard, *Photorefractive Materials and Their Applications* (Springer-Verlag, Berlin, 1988), Vol. 61.
[2] A. Ashkin, G. D. Boyd, J. M. Dziedzic, R. G. Smith, A. A. Ballman, J. J. Levinstein, and K. Nassau, Appl. Phys. Lett. **9**, 72 (1966).
[3] Y. S. Bai and R. Kachru, Phys. Rev. Lett. **78**, 2944 (1997).
[4] L. Hesselink, S. S. Orlov, A. Liu, A. Akella, D. Lande, and R. R. Neurgaonkar, Science **282**, 1089 (1998).
[5] K. L. Sweeney and L. E. Halliburton, Appl. Phys. Lett. **43**, 336 (1983).
[6] Y. Furukawa, K. Kitamura, S. Takekawa, A. Miyamoto, M. Terao, and N. Suda, Appl. Phys. Lett. **77**, 2494 (2000).
[7] G. Zhang and Y. Tomita, J. Appl. Phys. **91**, 4177 (2002).
[8] H. Mabuchi, E. S. Polzik, and H. J. Kimble, J. Opt. Soc. Am. B **11**, 2023 (1994).
[9] R. L. Townsend and J. T. LaMacchia, J. Appl. Phys. **41**, 5188 (1970).
[10] S. D. Setzler, K. T. Stevens, N. C. Fernelius, M. P. Scripsick, G. J. Edwards, and L. E. Halliburton, J. Phys.: Condens. Matter **15**, 3969 (2003).
[11] M. P. Scripsick, X. H. Fang, G. H. Edwards, L. E. Halliburton, and J. K. Tyminski, J. Appl. Phys. **73**, 1114 (1993).
[12] K. Buse, A. Adibi, and D. Psaltis, Nature (London) **393**, 665 (1998).
[13] P. Lerner, C. Legras, and J. P. Duman, J. Cryst. Growth **3/4**, 231 (1968).
[14] F. P. Safaryan, R. S. Feigelson, and A. M. Petrosyan, J. Appl. Phys. **85**, 8079 (1999).
[15] D. M. Smyth, Ferroelectrics **50**, 419 (1983).
[16] H. Donnerberg, S. M. Tomlinson, C. R. A. Catlow, and O. F. Schirmer, Phys. Rev. B **40**, 11909 (1989).
[17] Q. Li, B. Wang, C. H. Woo, H. Wang, and R. Wang, J. Phys. Chem. Solids **68**, 1336 (2007).
[18] O. F. Schirmer, H.-J. Reyher, and M. Wöhlecke, in *Insulating Materials for Optoelectronics-New Developments*, edited by F. Agulló-López (World Scientific, Singapore, 1995), pp. 93–124.
[19] C. Merschjann, D. Berben, M. Imlau, and M. Wöhlecke, Phys. Rev. Lett. **96**, 186404 (2006).
[20] O. F. Schirmer, O. Thiemann, and M. Wöhlecke, J. Phys. Chem. Solids **52**, 185 (1991); O. F. Schirmer, S. Juppe, and J. Koppitz, Cryst. Lattice Defects Amorphous Mater. **16**, 353 (1987).
[21] B. Faust, H. Müller, and O. F. Schirmer, Ferroelectrics **153**, 297 (1994).
[22] J. Koppitz, O. F. Schirmer, and A. I. Kuznetsov, Europhys. Lett. **4**, 1055 (1987).
[23] P. E. Blöchl, Phys. Rev. B **50**, 17953 (1994); G. Kresse and D. Joubert, *ibid.* **59**, 1758 (1999).
[24] G. Kresse and J. Hafner, Phys. Rev. B **47**, 558(R) (1993); **49**, 14251 (1994); G. Kresse and J. Furthmüller, Comput. Mater. Sci. **6**, 15 (1996); Phys. Rev. B **54**, 11169 (1996).
[25] S. L. Dudarev, G. A. Botton, S. Y. Savrasov, C. J. Humphreys, and A. P. Sutton, Phys. Rev. B **57**, 1505 (1998).
[26] *Ferroelectrics and Related Substances*, edited by K.-H. Hellwege and A. M. Hellwege, Landolt-Börnstein New Series,

Group III, Vol. 16 (Springer-Verlag, Berlin, 1981).
[27] Our calculated band gap is indirect: CBM at Γ point (0,0,0), and VBM at the region between Γ and *T* points $(1/2,1/2,1/2)$. However, we note that $LiNbO_3$ is approximately regarded as a direct band gap (Ref. 29) since the eigenvalue difference of Γ and VBM is very small, 0.02 eV.
[28] A. Dhar and A. Mansingh, J. Appl. Phys. **68**, 5804 (1990).
[29] W. G. Schmidt, M. Albrecht, S. Wippermann, S. Blankenburg, E. Rauls, F. Fuchs, C. Rödl, J. Furthmüller, and A. Hermann, Phys. Rev. B **77**, 035106 (2008).
[30] I. G. Austin and N. F. Mott, Adv. Phys. **18**, 41 (1969).
[31] O. F. Schirmer and D. von der Linde, Appl. Phys. Lett. **33**, 35 (1978).
[32] D. Berben, K. Buse, S. Wevering, P. Herth, M. Imlau, and Th. Woike, J. Appl. Phys. **87**, 1034 (2000).
[33] D. Emin, Phys. Rev. B **48**, 13691 (1993).